Article

Graphene Oxide and Adiponectin-Functionalized Sulfonated Polyetheretherketone with Effective Osteogenicity and Remotely Repeatable Photo-Disinfection

Yi Deng, Xiangyu Gao, Xiao-Lei Shi, Siyu Lu, Weizhong Yang, Chunyan Duan, and Zhi-Gang Chen

Chem. Mater., **Just Accepted Manuscript** • DOI: 10.1021/acs.chemmater.0c00290 • Publication Date (Web): 10 Feb 2020

Just Accepted

is published by the American Chemical Society. 1155 Sixteenth Street N.W., Washington, DC 20036

Graphene Oxide and Adiponectin-Functionalized Sulfonated Polyetheretherketone with Effective Osteogenicity and Remotely Repeatable Photo-Disinfection

Yi Deng[†,‡], Xiangyu Gao[†], Xiao-Lei Shi[⊥,#], Siyu Lu[&], Weizhong Yang[†,*], Chunyan Duan[^,*], Zhi-Gang Chen[⊥,#,*]

[†]College of Materials Science and Engineering, School of Chemical Engineering, State Key Laboratory of Polymer Materials Engineering, Sichuan University, Chengdu 610065, China

[‡]Department of Mechanical Engineering, The University of Hong Kong, Hong Kong SAR, China

[⊥] Centre for Future Materials, University of Southern Queensland, Springfield Central, Queensland 4300, Australia

[#]School of Mechanical and Mining Engineering, The University of Queensland, Brisbane, Queensland 4072, Australia

[&]College of Chemistry and Molecular Engineering, Zhengzhou University, Zhengzhou, 450001, China

[^]School of Basic Medical Sciences, Southwest Medical University, Luzhou 646000, China

ABSTRACT

Biomaterial-associated infection (BAI) is a serious threat to patients' health. In general, bacteriostatic agents are loaded on the surface of biomaterials to eliminate BAI; however, the excessive usage of these agents leads to the emergence of drug-resistant bacteria and inadequacy of tissue repair. To address this issue, here, we create a photo-responsive and osteopromotive coating that consists of graphene oxide (GO) nanosheets, polydopamine (pDA) nanolayers, and adiponectin (APN) protein on bioinert sulfonated polyetheretherketone (sPEEK/GO/APN). The functionalized samples display superior cytocompatibility and *in vitro* osteogenicity regarding cell reproduction, spreading, alkaline phosphatase activity, extracellular matrix calcification, and osteo-associated genes expression, outperforming sPEEK/GO and sPEEK/APN samples. The *in vivo* evaluation using a rabbit femur defect model demonstrates that the multifunctional coating significantly boosts bone regeneration and osseointegration. More importantly, the GO/pDA complex bonded together through π-π stacking and electrostatic interactions gives rise to robust cyclic photothermal bacteria-killing ability towards both Gram-positive and Gram-negative bacteria. Such a surface engineering platform may enable biomedical implants with enhanced osteogenetic ability and remotely recyclable photo-disinfection, holding great potential in the treatment of incurable infective bone loss.

1. INTRODUCTION

Owing to its excellent wear resistance, natural radiolucency, and similar mechanical property to human cortical bone, polyetheretherketone (PEEK) has gradually become the leading polymer material in the fields of orthopedics and trauma.[1] However, PEEK naturally lacks antibacterial ability, which significantly hampers the bone tissue growth.[2] Therefore, biomaterial-associated infection (BAI) has become a considerable issue since BAI is responsible for prolonged hospitalization periods, increased treatment costs, implant failure, and repeated surgeries.[3-5] Currently, antibiotic treatment is the main method to withstand bacteria invasion; however, subsequent biofilm formation makes the antibiotic therapy troublesome. Besides, the long-term abuse of antibiotics generates drug-resistance bacteria against most kinds of antibiotics[6, 7] and causes irreversible damage to some organs that detoxify the overdose of antibiotics.[8, 9] In this regard, great efforts have been devoted recently to create antibacterial implants that rely on the modification of bacteriostasis agents such as antibiotics,[10, 11] noble metal nanoparticles,[12, 13] antimicrobial polymers,[14-16] deoxyribonuclease (DNase) biomimetics[17, 18] onto implant surfaces. The general feature of these approaches is that the therapeutic effects are highly depended upon the intrinsic antibacterial ability of these loaded agents, called as "endogenous antimicrobial", which kills bacteria through antimicrobial agents on material surfaces, including drug loading, metal ions (Ag^{+}, Zn^{2+}, Cu^{2+}, etc.) delivery, or bacterial attachment resistance *via* electrostatic repulsion or super-hydrophobic surface. However, such "endogenous antimicrobial" approaches frequently necessitate much more time for bacteria disintegration, and are difficult to achieve the cyclic disinfection. Therefore, it is urgent to develop a novel "exogenous" strategy to combat bacteria/biofilm repeatedly and safely without bacterial resistance.

Light-assisted photothermal therapy (PTT) has captured considerable attention in the field of non-invasive treatment due to its unique merits, including low side effects, minimal invasiveness, deep tissue penetration, and highly effective bacteria-killing capability.[19, 20] Near-infrared (NIR) light-induced local hyperthermia for eradicating bacteria relied on photothermal conversion agents can kill bacteria through the destruction of biofilm structure, breakdown of membrane integrity, and denaturation of proteins/enzymes,[21-23] which does not cause drug-fast bacteria. In very recent decades, a variety of two-dimensional (2D) materials such as graphene oxide (GO)[24, 25], molybdenum disulfide (MoS_2),[26-28] manganese dioxide (MnO_2),[29, 30] black phosphorus,[31, 32] transition metal carbides/carbonitrides/nitrides (MXene)[33, 34] have been applied to eradicate bacteria owing to their outstanding near-infrared light (NIR) photothermal conversion efficiency. Ling et al. synthesized a GO-derived photothermal agent, Fe_2O_3 reduced GO modified by glutaraldehyde,[25] and found that the hyperthermal GO materials with temperature over 50 ℃ have an ability of efficient capture and killing of Gram-positive/Gram-negative germs under NIR light exposure. Although these 2D materials coatings can effectively improve the antibacterial properties of orthopedic implants, the light-induced hyperthermia can also cause the tremendous thermal injury of surrounding normal cells and healthy tissues around the implants, compromising their osteogenetic activity and osseointegration.

To tackle the challenge, herein, we designed and fabricated a multifunctional orthopedic material, consisting of PEEK material with GO nanosheet/polydopamine (pDA)/adiponectin (APN) hybrid coatings. Among these components, GO has a strong photothermal effect and excellent biocompatibility, which has been used in many biomedical areas.[35-37] Adiponectin (APN) is one of the amplest adipokine secreted by adipocytes. Its basic biological function is to maintain energy homeostasis and regulates glucose metabolism and fatty acid oxidation.[38] Currently, many

studies have shown that APN can serve as an active osteoinductive agent to facilitate osteogenic activity and induce *in vivo* bone formation.[39, 40] We used pDA binder, a substrate-independent and versatile surface modification strategy, to bond APN onto the GO surface. pDA is also a photothermal agent and can bond with GO together through π-π staking and electrostatic interaction. We envisage that our coating methodology will empower bioinert implants with tri-modal therapeutic functions: *in vitro* osteopromotive capability, elevated *in vivo* osteogenicity, and "on-demand" cycles of remote photo-disinfection.

2. EXPERIMENTAL SECTION

2.1. Preparation of GO and APN-Functionalized sPEEK

Medical-grade PEEK discs (450 G) with a size of *Φ* 8 × 3 mm was supplied from Victrex Ltd, (UK). These discs were immersed in concentrated sulfuric acid (97-99 wt%) to form the three-dimensional (3D) network on the PEEK surfaces. Ultrasonic agitation was applied throughout the entire process to obtain a uniform porous structure. After 5 min sulfonation, the treated samples were taken out and washed with deionized (D.I.) water through supersonic stirring to remove the remnant H_2SO_4. Afterward, the sulfonated PEEK (sPEEK) samples were first immersed in a 0.5 $mg \cdot mL^{-1}$ GO solution. After 20 min soaking, the samples were taken out and dried at 100 ℃ for 30 min. The process was repeated five times to immobilize GO onto the surface firmly. To graft APN protein, pDA was anchored onto the surface of GO-decorated sPEEK (sPEEK/GO) as described in previous literature,[41-43] through soaking the samples in 2 $mg \cdot mL^{-1}$ dopamine solution (in 10 mM Tris-HCl buffer with a pH of 8.5) for 6 hours (h). After rinsed with D.I. water, the pDA-grafted sPEEK was treated with 2 $\mu g \cdot mL^{-1}$ APN for 24 h at 4 ℃. The final sPEEK samples

(sPEEK/GO/APN) were then washed using D.I. water to remove the unattached APN protein and dried in air. The APN-modified sPEEK without GO interlayer (sPEEK/APN) and pDA-grafted sPEEK (sPEEK/pDA) were also prepared as control groups in this work.

2.2. Materials Characterization

We used field-emission scanning electron microscopy (FE-SEM, S-4800, Hitachi) and atomic force microscopy (AFM, SPA400, Seiko, Japan, a Si_3N_4 cantilever with a spring constant of 0.12 N/m) in the non-contact mode with 1.0 Hz scan rates to investigate the surface topology of prepared samples at various stages. Samples were vacuum-dried and coated by Au for SEM observation. The hydrophilicity of specimens in terms of water contact angle (WCA) was tested by a contact angle goniometry (SL200B, Kino). X-ray photoelectron spectroscopy (XPS, AXIS Ultra, Kratos) was applied to detect the chemical composition and elemental analysis.

2.3. Photothermal Effect

The temperature of the samples should rise under 808 nm NIR laser, so the photothermal property was measured and captured using a thermal infrared camera (FLIR, E6, USA). All samples were immersed in 500 μL PBS solution and then put into the 48-well plates. Samples were exposed under an 808 nm laser illumination at 0.5 $W \cdot cm^{-2}$ for 10 min and cooled down spontaneously for another 10 min. We recorded the temperature change every 1 min. In the photothermal circle test, the temperature was recorded every 1 min.

2.4. Deposition of Bone-Like Apatite

The 1X SBF solution (**Table S1**) was fabricated by dissolving NaCl, $NaHCO_3$, KCl, $K_2HPO_4 \cdot 3H_2O$, $MgCl_2 \cdot 6H_2O$, $CaCl_2$, and Na_2SO_4 in order in D.I. water and buffering to pH = 7.4 using $(CH_2OH)_3CNH_2$ and 1 $mol \cdot L^{-1}$ HCl at 37 ℃.[44, 45] These functionalized sPEEK samples were

immersed in this solution at 37 ℃, and after 1 and 2 weeks immersion, sPEEK samples were taken out from SBF and rinsed by D.I. water. Finally, the microstructures of calcium nodules on sample surfaces were determined by SEM.

2.5. Cell Experiments

2.5.1. Cell Cultivation and Seeding

Mouse osteoblast precursor cells MC3T3-E1 were cultivated in cell culture media containing Dulbecco's modified Eagle's media (DMEM, Gibco), 10 % fetal calf serum (Hyclone, USA), and 1 % penicillin/streptomycin (Hyclone). Afterward, these cells were seeded onto the sPEEK samples in 48-well plates with a density of 4×10^4 cells/well. Cell media were refreshed every 2 days.

2.5.2. Cell Activity and Cytotoxicity

The cell proliferation and survival of cells on various sPEEK samples were tested with a Cell Counting Kit (CCK-8, Dojindo, Japan) and Lactate Dehydrogenase Kit (LDH, KeyGEN BioTECH, Jiangsu) per the manufacturer's instructions. In the CCK-8 test, after 1, 3, and 5 days of culturing, the media was mixed with 10 % CCK-8 reagent. After 3 h of reaction, 100 μL of supernatant from each sample was introduced into a fresh 96-well plate, and the absorbance of solution (OD) at λ = 450 nm was measured using a Microplate reader (SAF-6801, BAJIU). With regard to LDH assay, the media was collected and centrifuged, and the diluted supernatant (1:25) was reacted with LDH working solution and incubated at 37 ℃ for 0.5 h. The results were quantified at λ = 440 nm using the same reader.

2.5.3. Cell Morphology and Cytoskeleton Staining

Cells at 1 day on samples were fixed using 2.5 % glutaraldehyde for 3 h and next dehydrated in ascending ethyl alcohol (40, 60, 70, 90, 95, 100 %) for 20 min each gradient. Afterward, cells were vacuum-dried in critical point drying, coated with Au, and detected by FE-SEM.

2.6. *In Vitro* Osteogenicity

After 2 days of incubation, the cell culture media was substituted by the osteoinductive media containing 100 nM dexamethasone, 50 $\mu g \cdot mL^{-1}$ ascorbic acid, and 100 mM β-glycerophosphate to induce the osteogenic commitment of MC3T3-E1 osteoblasts. The cell media were refreshed every 2 days.

2.6.1. Alkaline Phosphate Activity

We first applied an alkaline phosphate (ALP) activity assay kit (Nanjing Jiancheng Biotechnology) to evaluate intracellular ALP activity of cells cultured on various samples after 7 and 14 days of cultivation. Briefly, cells were lysed using Triton X-100 (1 % v/v). The cell-lysis solution was collected and then 30 μL supernate was reacted with ALP working solution according to the manufacturer's guidance. Finally, the OD value of the mixed solution was tested at 520 nm by a microplate reader. Then, a Micro-BCA protein assay kit (KeyGEN BioTECH, Jiangsu) was employed to quantify the total protein amount. Furthermore, the ALP distribution on sPEEK scaffolds was visualized by a BCIP/NBT ALP color development kit (Beijing ComWin Biotech).

2.6.2. Alizarin Red S Staining

Alizarin Red S (ARS) staining was used to estimate the calcified deposition by cells in the osteoinductive media at day 21. Briefly, cells with scaffolds were fixed in 4 % paraformaldehyde for 40 min. ARS solution (2 %, pH = 4.2, Sigma) was then incorporated into each well containing samples for 1 h incubation. Redundant ARS dye was removed using D.I. water, and the formed

calcium deposition was recorded by a scanner. To quantify the calcium amount, the ARS-stained samples were reacted with 20 % cetylpyridinium chloride, and then the absorbance of extracts was detected using the reader at a wavelength of 570 nm.

2.6.3. Real-Time PCR

After 14 days of induction in osteoinductive media, the total mRNA of cells was isolated by TRIzol (Invitrogen) and transformed into cDNA with the RevertAid First Strand cDNA Synthesis Kit (Thermo) following the manufacturer's guidance. Real-time polymerase chain reaction (RT-PCR) analysis was conducted using the ABI 7500 real-time PCR machine (Applied Biosystems) using SYBR Green (Roche). The primers (5′-3′) used in this study were listed in **Table S2**.

2.7. *In Vivo* Osteogenesis Assessments

All procedures were authorized by the Animal Ethics Committee at Southwest Medical University. Forty-eight sPEEK implants (Φ 4 × 8 mm) were randomly assigned to four groups: sPEEK control (n = 6), sPEEK/GO (n = 6), sPEEK/APN (n = 6), and sPEEK/GO/APN implants (n = 6). Before the operation, general anesthesia was conducted on twenty-four 2-month-old New Zealand white rabbits (2.6-3.2 kg) through intravenous injection of 4 % pentobarbital sodium (50 mg·kg^{-1}). Two bone defects whose size matched those of implants were created on a bilateral femur using a dental trephine. The cylinders were implanted into the created holes on each side of the femur, followed by step-by-step suture and incision closure[46]. To label the neo-tissue formation process, 40 mg·kg^{-1} calcein was intravenously injected into animals at 2 weeks. The rabbits suffered intramuscular injection of penicillin sodium (40 U·kg^{-1}) for 4 days post-operation and were sacrificed at 4 and 8 weeks. The harvested tissues containing internal implants were fixed in 10 % formalin for follow-up assessments.

2.7.1. Micro-CT Analyses

We used Micro-CT to scan the fixed femurs containing implants, and 3D models were reconstructed through equipped software (Scanco Medical vivaCT40, Switzerland). Afterward, the trabecular bone volume/tissue volume (BT/TV), trabecular number (Tb.N), trabecular thickness (Tb.Th), and trabecular spacing (Tb.Sp) were also quantified.

2.7.2. Histological Evaluation

The undecalcified tissues were dehydrated with a prepared gradient alcohol solution and then embedded in methyl methacrylate resin. Afterward, the samples were cut into 80 μm sections using a microtome (RM2125, Leica) for toluidine blue-fuchsine staining to observe regenerated bone tissues. Moreover, these sections were used to capture the fluorochrome signal using a confocal laser scanning microscope (CLSM, A1R MP+, USA). And the implant surfaces after separating the samples from the underlying tissue were observed by SEM.

2.8. Remote Antibacterial Tests

In the present work, we employed *Staphylococcus aureu*s (*S. aureu*s, Gram-positive) and *Escherichia coli* (*E. coli*, Gram-negative) as two model microbes to evaluate the antimicrobial performances of the coated sPEEK samples. Bacteria were cultivated in Luria-Bertani (LB) media, and antimicrobial ability was tested through the spread plate method, SEM observation, and Live/Dead staining.

For repeated antibacterial tests, samples were first sterilized using 75 % ethanol solution for at least 30 min. 200 μL bacterial suspension ($1 \times 10^{6\text{-}8}$ CFU·mL^{-1}) was introduced into each well (48-well plate) with these studied materials, and they were exposed under an 808 nm light for 20 min with a power density of 0.5 W·cm^{-2}. Then the spread plate approach was used to evaluate the

antibacterial efficiency. Briefly, bacteria attached to all samples were detached through vortex for 10 min. After 100 times dilution of the bacterial solution from corresponding samples, 40 μL bacterial suspension was evenly coated on the LB agar in a Petri dish as the first antibacterial test. These samples were collected again and immersed in PBS at 37 °C for 1 days. After that, samples were used to repeat the above antibacterial test twice. We counted the number of colonies on the LB agar after 1 day of incubation, and the antibacterial efficiency was calculated following the equation:

$$\text{Antibacterial efficiency} = (N_{control}\text{-}N_{sample})/N_{control} \times 100\ \%$$

Where $N_{control}$ is the amount of colonies in sPEEK control, and N_{sample} is the amount of colonies in other groups.

With regard to Live/Dead staining, the adhered bacteria onto the sPEEK samples were stained using a Live/Dead BacLight bacteria viability kits (Thermo Fisher, USA). Then samples containing bacteria were washed with PBS and observed using CLSM. The morphological alteration of bacteria and their membranes were captured by SEM. After the NIR illumination for 20 min, bacteria on samples were fixed using 2.5 % glutaraldehyde, followed by dehydration with a gradient alcohol solution (30-100 %, each step for 120 min). After dried at ambient temperature, morphologies of bacterial body and membrane were captured by SEM.

2.9. Statistical Analysis

For quantification, at least five samples for each group were tested to provide the mean ± standard deviation. We used One-way ANOVA and Tukey's post hoc tests through SPSS 19.0 software to determine the significant differences.

3. RESULTS AND DISCUSSION

3.1. Design and Characterization of GO/pDA/APN-Decorated sPEEK

Scheme 1 illustrates the preparation of the GO/pDA/APN-decorated sPEEK and its multi-modal therapeutic effects, including *in vitro* osteogenicity, *in vivo* bone regeneration, and non-invasive "exogenous" photo-disinfection. 3D networks are constructed on the surface of sPEEK to facilitate the tissue in-growth and provide reservoirs for drugs.[47] Then, two layers of GO and pDA are bonded onto sPEEK samples by π-π-π stacking and electrostatic interactions. In this work, pDA nanolayer serves as an anchor to covalently tether APN protein *via* thiols and amines due to Schiff-base and Michael-addition reactions, giving rise to a multilayer nano-coating. **Figure 1(a-b)** depicts the surface topologies of these surfaces before and after functionalization. The bare sPEEK has a 3D network structure, while a porous structure is fully covered by GO membrane after GO deposition. Furthermore, the immobilization of pDA and APN somewhat increases the surface roughness of GO with numerous pDA nanoparticles. However, in sPEEK/APN sample, only APN protein decoration cannot alter its 3D porous morphology, verified in AFM images. As can be seen, micro-pores exist on the surfaces of sPEEK and sPEEK/APN, and their roughness slightly reduces after GO decoration. It is well-accepted that WCA can track and estimate the effectiveness of surface modification protocols. The measured WCA of our samples are shown in **Figure 1(c**). As can be seen, the sPEEK surface displays hydrophobic nature with a WCA of ~78°. After GO modification, WCA alters to 50.10 ± 2.65°, while WCA of sPEEK/GO/APN is 24.67 ± 1.53° indicating a hydrophilicity, which is attributed to the hydrophilic nature of pDA coating and APN protein.[48]

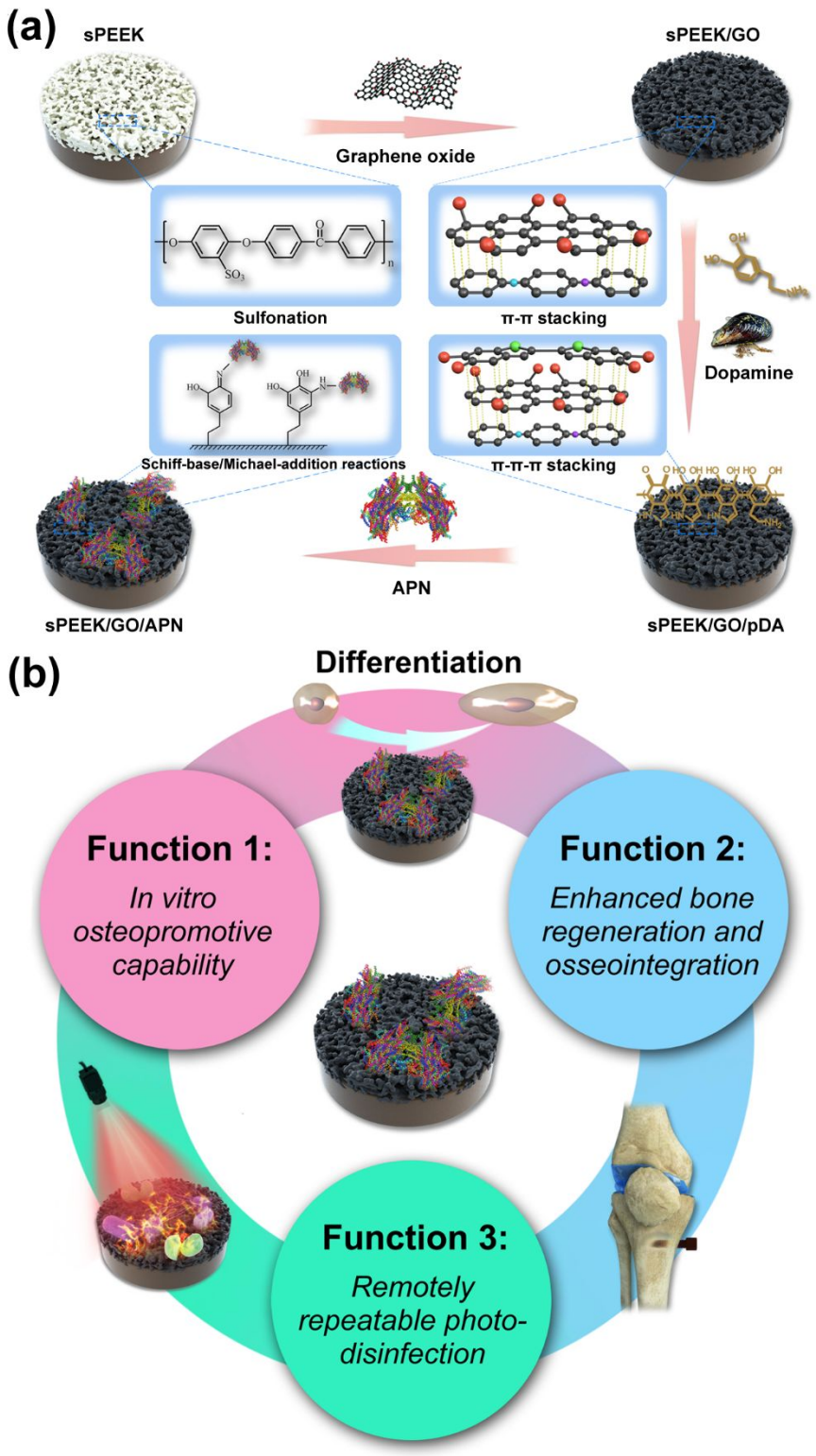

Scheme 1. (a) Schematic illustration of the fabrication of the multifunctional sPEEK and (b) its triple-model therapeutic effects.

Figure 1(d-e) shows the XPS full spectrums and slow-scan spectrums of our samples, which display chemical constituents of the multifunctional hybrid coatings. In the full spectrum of sPEEK, C, O, and S are the primary elements, in which S element comes from sulfonation. The suppressed intensity of S 2p signal and the appearance and enhanced intensity of N 1s signal indicate the successful decoration of GO and APN (**Figure 1(d)**). Furthermore, the high-resolution carbon spectra (C 1s) are provided in **Figure 1(e)**. The high-resolution C 1s spectra of sPEEK and sPEEK/GO samples are deconvoluted into three sub-curves. The binding energies at 284.5, 286.3, and 287.9 eV are associated with the carbon skeleton (-C-C-/-C-H-), hydroxyl group (-C-O) and carbonyl group (-C=O), respectively. Compared with sPEEK, the peak intensity of -C-O and -C=O groups for sPEEK/GO increases and attributes to the presence of GO nanocoating. A broad peak belonged to -C-N- signal appears at ~284.9 eV for sPEEK/APN and sPEEK/GO/APN samples, indicating the successful tethering of APN.

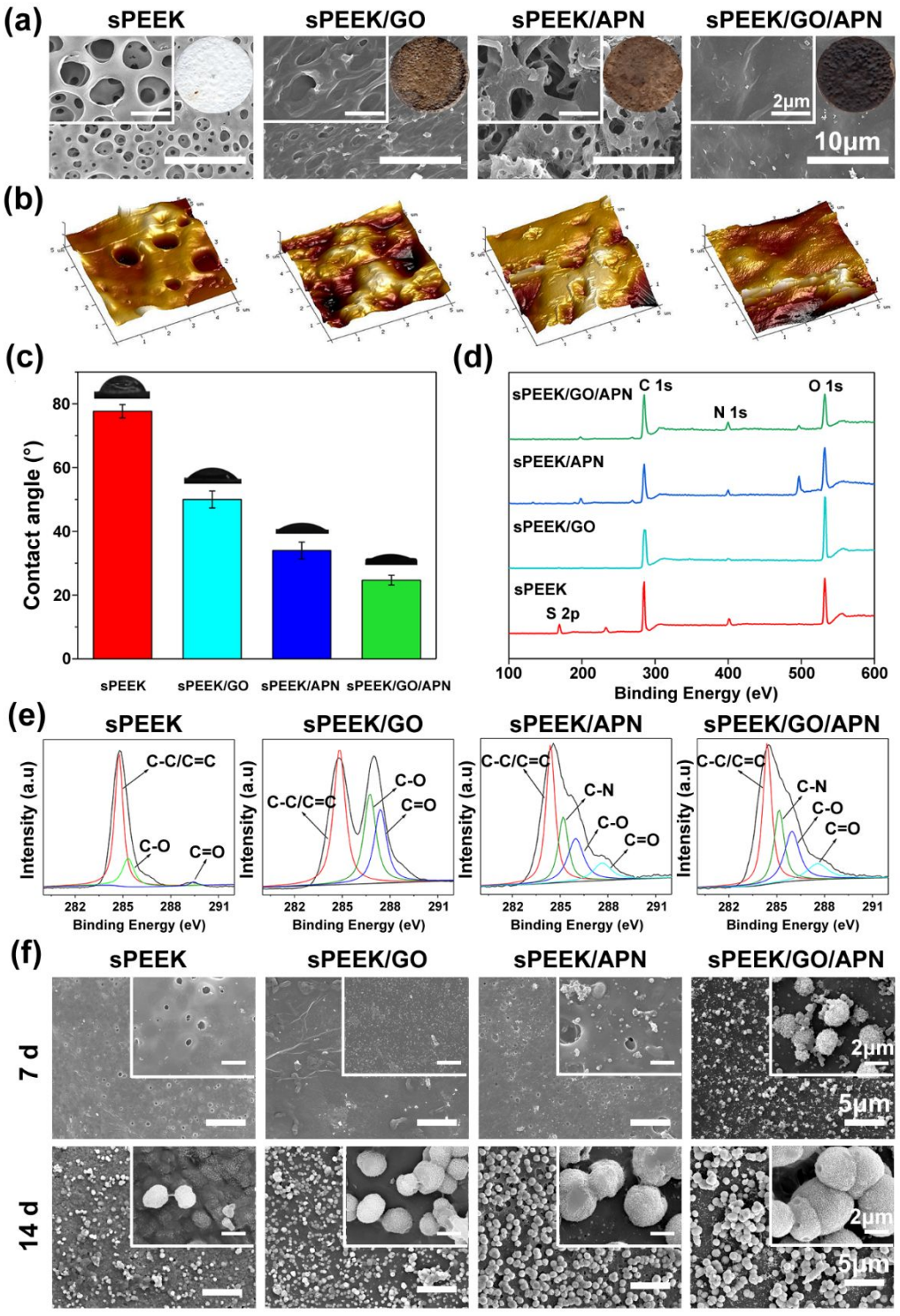

Figure 1. Characterization of GO/pDA/APN hybrid coating on sPEEK surfaces: (a) Optical, SEM, and (b) AFM images for surface morphology; (c) Water contact angle, (d) XPS survey and high-

resolution spectra of C1s of different multifunctional sPEEK. (f) SEM observation of bone-like apatite nodules on multifunctional sPEEK samples after soaking in SBF solution.

3.2. Formation of Bone-Like Apatite Deposition

One of a significant symbol of bioactive implants is their capability to integrate with surrounding bone tissue;[44] hence, the formation of bone-like apatite deposition on their surface was further investigated. As illustrated in **Figure 1(f)**, no Ca-P sediments form for sPEEK and sPEEK/GO at the beginning of 7 days, but many spherical apatites appear after 2 weeks of immersion. In sharp contrast, a handful of clustered nodular aggregations emerge on sPEEK/APN and sPEEK/GO/APN surfaces after 1 week. While when the time extends to 2 weeks, the number of precipitates dramatically increase. Among these groups, sPEEK/GO/APN induces the largest quantity of bone-like apatite deposition on the surface, indicating that *in vitro* bioactivity of the hybrid coating is much better than that of single GO or APN coating.

3.3. Photothermal Effect

A real-time photograph on the evolution of the surface temperature is recorded when the samples are illuminated under 808 nm laser with a power of 0.5 W/cm^2 and the results are shown in **Figure 2(a)**. Infrared thermal images indicate that after GO and pDA coating, sPEEK/GO, sPEEK/pDA, sPEEK/APN, and sPEEK/GO/APN samples all present the photothermal effect to some extent, while no apparent photothermal effect can be observed on sPEEK samples. To determine whether GO or pDA becomes a major factor for photothermal generation, we compared the photothermal effect of sPEEK/GO with sPEEK/pDA. As shown in **Figure 2(b)**, sPEEK/pDA shows a lower photothermal effect achieving 39.8 °C; however, the highest hyperthermia temperature of sPEEK/GO reaches 48.7 °C within 10 min, indicating GO coating has a stronger photothermal

effect than pDA coating. Compared with sPEEK/GO and sPEEK/pDA, sPEEK/GO/APN displays a higher temperature (yielding 50.4 °C) and a faster heating rate (i.e., a high photothermal effect). This is because the synergy of GO/pDA complex held together through π-π interaction generates a robust photothermal effect. **Figure 2(c)** shows the temperature elevating and cooling profiles of sPEEK/GO/APN samples. We can see that there is no noticeable difference in temperature rising and cooling process among three cycles, illustrating that the thermal stability of the GO/pDA/APN hybrid coating is excellent.

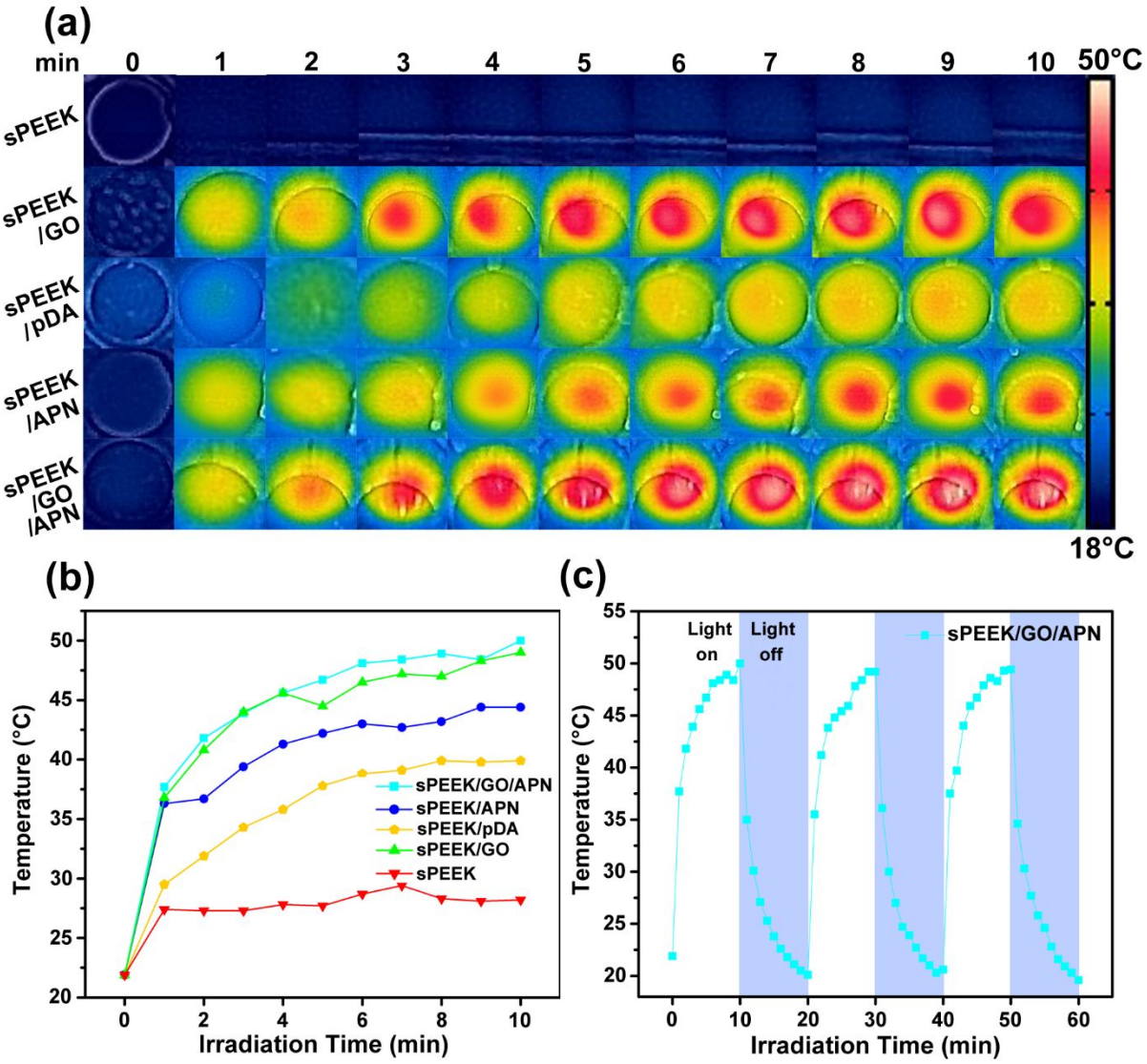

Figure 2. Photothermal property tests of different sPEEK samples irradiated by 808 nm light with a power density of 0.5 $W \cdot cm^{-2}$: (a) Infrared thermal images of samples; (b) Photothermal heating curve of samples; (c) Temperature rising and cooling cycles of sPEEK/GO/APN.

3.4. Cytocompatibility Assessments

After *in vitro* bioactivity tests, we further investigated the effect of multifunctional sPEEK on the cell reproduction, cytotoxicity, and spreading of MC3T3-E1 cells, an osteoblast precursor cell line. The results of cell viability and cytotoxicity detected by CCK-8 and LDH kits are shown in **Figure 3(a-b)**. After cultivated with MC3T3-E1 for 3 and 5 days, higher cell proliferation is detected in sPEEK/GO than sPEEK in line with much previous literature that GO can support cell proliferation and accelerate osteogenic differentiation.[37, 49] Because of the excellent biocompatibility of APN protein, sPEEK/GO/APN exhibits the most significant cell proliferation. Besides, the test of LDH enzyme release was carried out, which is an indicator of cytotoxicity. Although the vales of LDH release drop with time, lower LDH activity is found in sPEEK/GO/APN than that in sPEEK and sPEEK/GO samples at both 3 and 5 days, indicating low cytotoxicity (**Figure 3(b)**).

Figure 3(c) shows an overview of the morphologies of MC3T3-E1 cells on samples captured by SEM. Poor cell attachment with fusiform shape is observed in sPEEK samples, and it may be ascribed to the residual of sulfuric acid in the pore after sulfonation.[50] However, cells in sPEEK/GO show a larger area of cell spreading. Notably, the most considerable quantity of cells is seen on sPEEK/APN and sPEEK/GO/APN samples, and these cells present more extended filopodia than those on sPEEK/GO. These results demonstrate that the hybrid coating on sPEEK samples is capable of facilitating proliferation and spreading, showing good cytocompatibility.

3.5. *In Vitro* Osteogenicity Evaluations

To understand the osteogenic potential of the GO/pDA/APN decoration, ALP activity, calcium-related extracellular matrix (ECM) secretion, and osteogenesis-associated genes expression were measured. **Figure 3(d)** shows the ALP production of MC3T3-E1 on the surfaces of our samples, as an early hallmark for osteoblastic differentiation. Compared with sPEEK, sPEEK/GO shows higher ALP activity at both 7 and 14 days owing to the osteoconductive nature of GO.[49, 51] Furthermore, after APN decoration, larger quantities of ALP production are detected in sPEEK/APN and sPEEK/GO/APN samples than those in sPEEK and sPEEK/GO samples, suggesting that APN protein has a stronger osteoinductive ability than GO nanosheets.

The mineral ECM secretion, being an inherent feature of bone-like structures, was further evaluated as osteogenic biomarkers at the late stage of osteogenic differentiation. Higher areas of dark red color are detected on two APN-tethering sPEEK (sPEEK/APN and sPEEK/GO/APN) samples from ARS staining for calcium-related ECM deposition, consistent with ALP activity results. This result indicates that the secreted ECM is calcified by differentiating osteoblasts. Recently, APN has been demonstrated to augment osteogenic differentiation *via* activating Wnt/β-catenin and APPL1-AMPK signal pathways.[38, 52] Further, a quantitative analysis of ARS staining in **Figure 3(e)** corroborates the foregoing stain results that sPEEK/GO/APN has induced the largest amount of calcium deposition due to the presence of the osteoinductive APN protein.

We further detected the expression of osteo-associated genes, including RUNX2, OCN, and COL1A1 in MC3T3-E1 co-cultivated on the multifunctional sPEEK samples (**Figure 3(f)**). There is no difference between sPEEK and sPEEK/GO in three osteogenesis-associated genes. However, the hybrid coating consisted of APN and/or GO nanosheets significantly facilitate MC3T3-E1 commitment to the mature osteoblasts. These data have disclosed that sPEEK/GO/APN has a

superior capability in promoting *in vitro* osteoblastic maturation resulting from the synergistic action of GO nanosheets and APN protein.

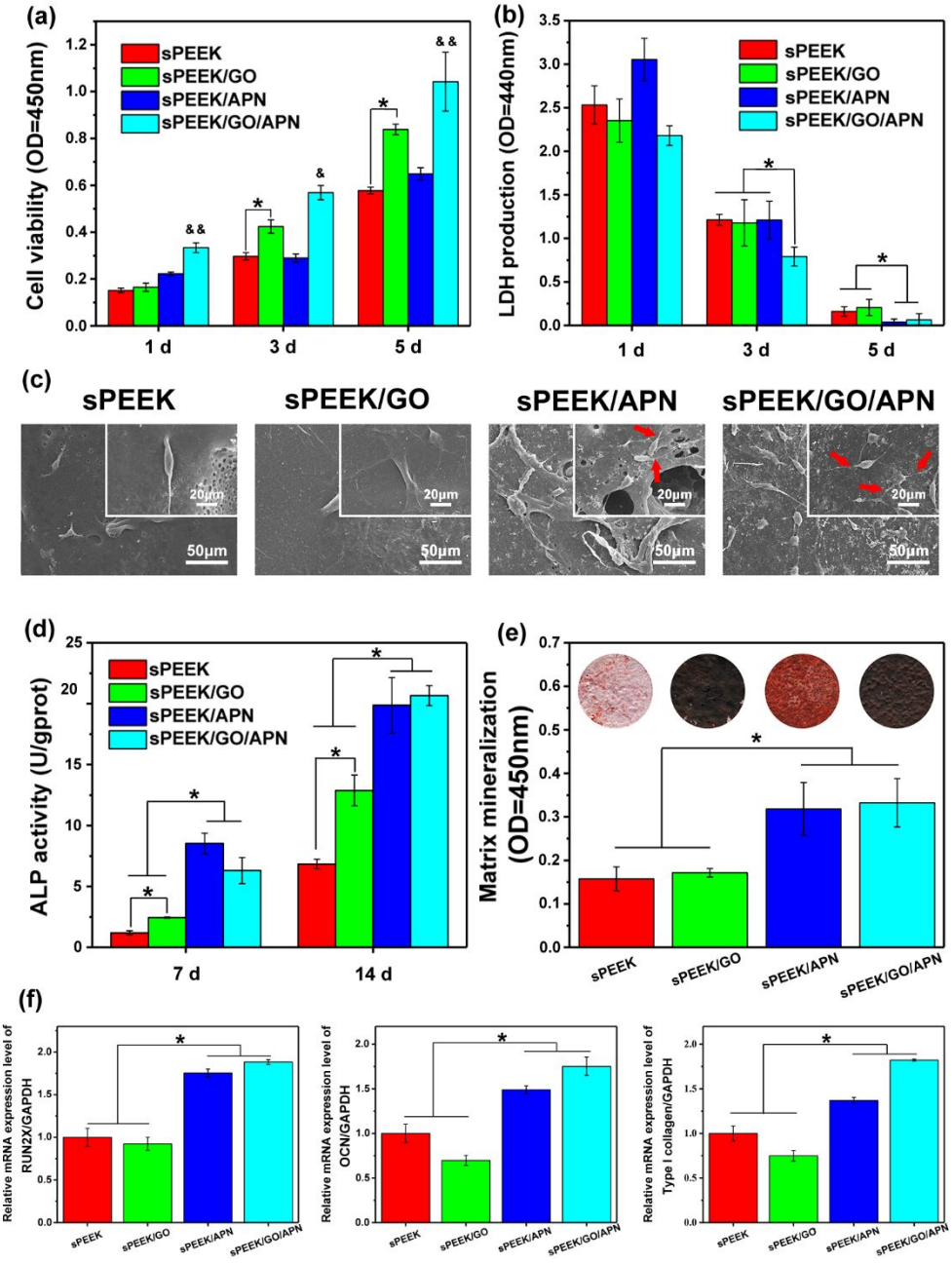

Figure 3. *In vitro* cytocompatibility and osteogenesis evaluations: (a) Cell proliferation, (b) LDH enzyme activity, and (c) Cell morphology of MC3T3-E1 on the samples. Red arrows reveal the extended pseudopod; (d) ALP activity, (e) Coloring and quantification of ARS staining for calcium

nodules, and (f) RT-PCR results for osteogenesis-related genes on multifunctional sPEEK. & represents $p < 0.05$ compared to other groups, && represents $p < 0.01$ compared to other groups, * represents $p < 0.05$ between groups.

3.6. *In Vivo* Osteogenesis

The *in vitro* cell test results guide us to estimate the *in vivo* tissue responses of these multifunctional implants through an animal model. Therefore, a New Zealand rabbit femur defect implantation model was used for a demonstration of *in vivo* osseointegration and bone regeneration. Different functionalized sPEEK implants were implanted into the femoral marrow cavity, and we assessed neo-tissue formation at 4- and 8-week post-surgery using μ-CT, histological analyses, and fluorescent labeling. At 4- and 8-week, the animals were sacrificed, and femurs were taken out for X-ray detection, as shown in **Figure S1**. The optical and X-ray images show that the implants bond with bone tissue well, and there is no inflammation symptom. **Figure S2** and **Figure 4(b)** present the 2D and 3D micro-CT images of the new-tissue adjacent to implants, respectively. The high-resolution scans clearly exhibit discontinuous parts of bone around sPEEK implants, and more formation of newborn osseous tissue is found around sPEEK/GO and sPEEK/APN implants. Moreover, the implanted sPEEK/GO/APN implants are surrounded by the most quantity of bone at both 4 and 8 weeks among groups, demonstrating its outstanding *in vivo* osseointegration. The quantitative analyses of bone histomorphometry indices are provided in **Figure 4(c)**. The BV/TV and Tb.Th for sPEEK/APN implants are dramatically higher than those for sPEEK. Notably, sPEEK/GO/APN displays the highest BV/TV, Tb.Th and Tb.N combined with lowest Tb.Sp among groups after 8 weeks of post-surgery. The results demonstrate that sPEEK implants with the dual GO and APN functionalization dramatically boost new osseous tissue formation than other sPEEK controls, which corresponds to the reproduction and osteoblastic potential of cells *in vitro*.

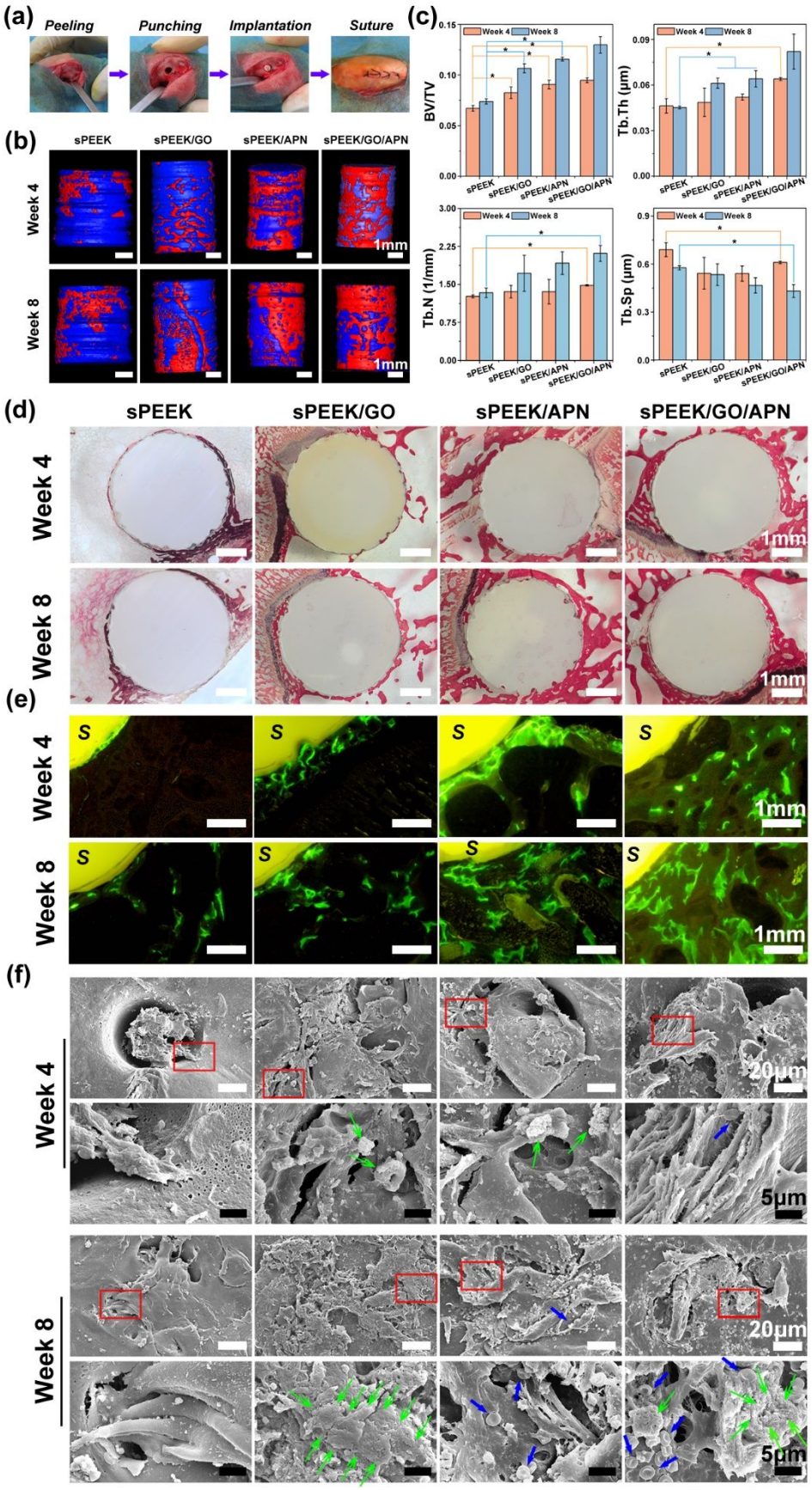
(a)
Peeling
Punching
Implantation
Suture
(b)
sPEEK
sPEEK/GO
sPEEK/APN
sPEEK/GO/APN
Week 4
Week 8
1mm
(c)
Week 4
Week 8
BV/TV
Tb.Th (μm)
Tb.N (1/mm)
Tb.Sp (μm)
(d)
sPEEK
sPEEK/GO
sPEEK/APN
sPEEK/GO/APN
Week 4
Week 8
1mm
(e)
S
Week 4
Week 8
1mm
(f)
Week 4
Week 8
20μm
5μm

Figure 4. *In vivo* osteogenesis assessments: (a) The surgical step of rabbit femur implantation. (b) Reconstructed micro-CT 3D models and (c) Corresponding bone histomorphometry of different multifunctional sPEEK implants at Week 4 and 8. (d) Histological assessment of the undecalcified sections stained with toluidine blue-fuchsine staining to demonstrate the *in vivo* osseointegration of the multifunctional sPEEK implant surfaces. (e) Fluorescent labeling of new bone regeneration around the sPEEK implants. Green represents labeling by calcein. *S*: Sample. (f) SEM observation of bone attachment and ingrowth to the implant surfaces following the separation of implants from the animals. The red box shows the zoom view of the images. Blue arrows point to hemocytes, and green arrows indicate the calcified matrix. * and ** represents $p < 0.05$ and $p < 0.01$ between groups; # represents $p < 0.05$ compared to other groups at Week 8.

We next used histological staining to identify the newly-regenerated bone around implants. Toluidine blue-fuchsine staining in **Figure 4(d)** shows very few bone fragments attached to sPEEK implant surface. However, an augmented amount of new bone is found around sPEEK/GO at 8 weeks, and APN functionalization (sPEEK/APN) significantly improves bone formation around implants at both 4 and 8 weeks. It should be noted that new bone firmly anchors onto the sPEEK/GO/APN surface and extends along with the whole implant interface, showing the most amount of new-regenerated bone. The fluorochrome assays further validate the micro-CT results. More green fluorescence is detected around the sPEEK/GO/APN implants (**Figure 4(e)**), which is an indicator of a more calcified matrix. Hence, the histological staining and fluorescent labeling results both suggest that the GO/APN co-functionalization induces newly-formed bone.

Figure 4(f) shows SEM photographs of the implant surfaces after separating the implants from the underlying tissue. As can be seen, only a handful of bone tissues are bonded to the surface of

sPEEK implants, whereas some calcified matrix is found in sPEEK/GO and sPEEK/APN implants at 4 weeks. When the time extends to 8 weeks, more bones attach onto all the samples. Newly-formed bone tissues attempt to grow into the pore on the surface of sPEEK implants, in line with the previous studies that porous structure facilitates bone ingrowth.[53] We can also see a mass of calcified matrix in the sPEEK/APN samples, suggesting APN has a strong capability to induce apatite deposition *in vivo*, consistent with the *in vitro* bone-like apatite formation test (**Figure 1(f)**). Remarkably, sPEEK/GO/APN surface is fully covered by the regenerated calcified bone and hemocytes. The appearance of abundant hemocytes indicates that plentiful blood supply can accelerate bone reconstruction and remodeling. Overall, these *in vivo* results have demonstrated that GO and APN co-treatment not only dramatically promotes bone regeneration but also stimulates revascularization around implants.

3.7. Remotely Repeatable Antibacterial Performances

Biomaterial-associated infection caused by bacteria and its repeated infection syndrome is one of the most prevalent complications after surgery. As an efficient approach for disinfection, light-assisted PTT has been extensively investigated in antibacterial therapy. Here, the photothermal antibacterial properties of the multifunctional sPEEK samples and their repeatable sterilization efficacy against two bacterial models *S. aureus* and *E. coli.* under the illumination of 808 nm NIR laser were studied. As shown in **Figure 5(a)**, all samples have no antibacterial activity without light, and bacteria reproduce well with negative antibacterial efficiency on sPEEK/APN and sPEEK/GO/APN (**Figure. S3**), because APN protein can provide nutrition for bacterial growth. After irradiation under light for 20 min, there is a little reduction of colonies on sPEEK/GO and sPEEK/APN samples due to the certain photothermal effect of GO and pDA nanolayers, respectively. However, only a shade of colonies survives in sPEEK/GO/APN samples after

illumination for 20 min. The order of antimicrobial rates is sPEEK/GO/APN > sPEEK/GO > sPEEK/APN > sPEEK, and the antimicrobial efficiencies of sPEEK/GO/APN against *S. aureus* and *E. coli* achieve approximately 99.49 % and 92.40 %, respectively. This is because the high temperature produced by the synergistic effect of the GO/pDA complex under 808 nm light kills the bacteria, which is demonstrated by photothermal properties tests (**Figure 2**). After the first antimicrobial test, these used samples were immersed in PBS for 1 day and suffered second and third antimicrobial tests. **Figures S3-S4** reveal that sPEEK and sPEEK/APN have no recyclable antibacterial property. However, sPEEK/GO/APN displays repeatable antimicrobial rates over 93 % against *E. coli* and *S. aureus* (**Figure S3**), and there are only a few bacterial colonies in sPEEK/GO/APN samples, even after a ternary cycle of photo-disinfection operation (**Figure 5(b)** and **Figure S4**). These results demonstrate that GO/pDA complex can produce robust cyclic photonic antimicrobial effects.

We used Live/dead staining assay to assess the anti-biofilm ability of the multifunctional samples, and the corresponding fluorescent images of the biofilm are shown in **Figure 6(a)**. Without light irradiation, sPEEK and sPEEK/APN are entirely stained with green (alive bacteria), indicating that the surfaces are favorable for bacterial proliferation. And there are lower amounts of alive bacteria on sPEEK/GO and sPEEK/GO/APN samples in the absence of light because GO nanosheets have a certain antimicrobial function through biofilm prevention/anti-adhesion. After irradiation under 808 nm light for 20 min, sPEEK samples show similar fluorescence to the samples cultivated in the dark, implying the whole active biofilm on the surface. Fewer green fluorescence with declined bacteria amount is detected on the surface of sPEEK/APN due to the photothermal effect of pDA coating. In striking contrast, there is nearly no fluorescence on the surface of sPEEK/GO/APN samples, indicating GO/pDA/APN hybrid coating exerts a good

ability to prevent the biofilm produced by bacteria, which is in accordance with the results from spread plate experiments.

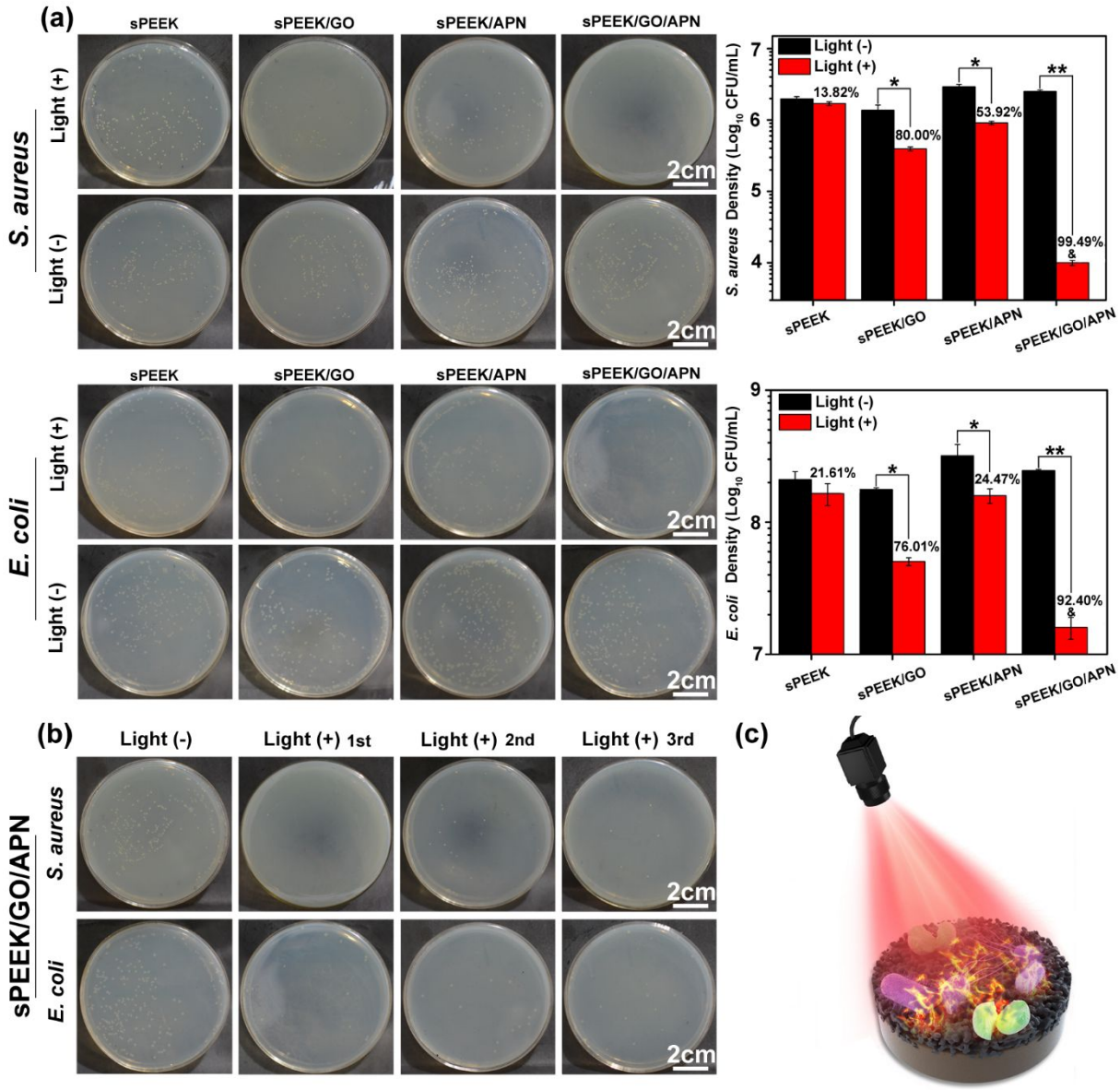

Figure 5. Antibacterial activities of multifunctional sPEEK samples after NIR exposure or in the dark for 20 min: (a) The spread plate method with sterilization efficiency. (b) The recyclable antimicrobial tests of sPEEK/GO/APN samples. (c) Schematic illustration of the photothermal effect for the killing of bacteria. && represents $p < 0.01$ compared to other groups, * represents $p < 0.05$ between groups, and ** represents $p < 0.01$ between groups.

The morphologies and membrane integrity of the bacteria attached to the coatings were also tested using FE-SEM (**Figure 6(b)**). The bacteria on all samples in the dark display healthy and intact spherical and rod shapes, respectively, implying no antibacterial performance. After illumination, the *S. aureus* and *E. coli* on sPEEK and sPEEK/APN samples also show compact morphology with a smooth and integrated membrane. After exposed under NIR laser for 20 min, bacteria on sPEEK/GO and sPEEK/GO/APN samples are possibly suffered from damage. For instance, *S. aureus* displays lytic membranes and cytoplasmic leakage (shown in the green ellipses and arrows), while *E. coli* shows irregular shape and shrinking body (pointed by red arrows). The phenomenon deteriorates on sPEEK/GO/APN samples. These results reveal that the hybrid coating may have a robust, recyclable photo-disinfection property for both Gram-positive/Gram-negative bacteria under NIR light.

When the implants stay in the human body for a long time, they are susceptible to bacterial contamination, leading to biomaterial-associated repeated infection (BARI) syndrome. The conventional approaches rely on antibacterial agents-impregnated implants. They kill bacteria through bactericides on material surfaces, including drug loading, metal ions (Ag^{+}, Zn^{2+}, Cu^{2+}, etc.) delivery, or bacterial attachment resistance *via* electrostatic repulsion. However, their antibacterial performances are often controlled by the body itself, and it is challenging to achieve cyclic disinfection. The significance of the work is that the repeatable photo-disinfection performances of our coating manipulated by remote light can effectively eliminate the BARI without administering antibiotics.

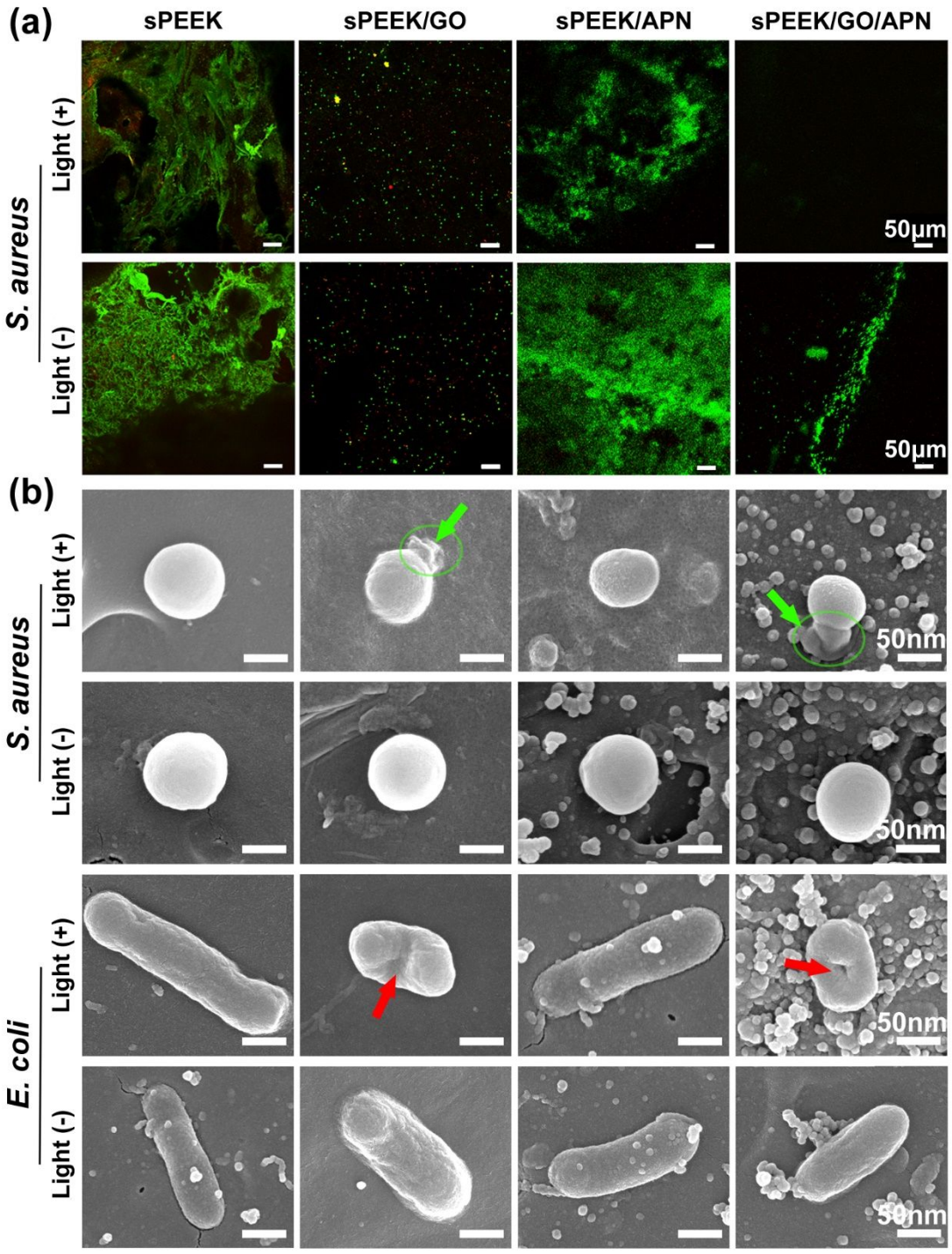

Figure 6. (a) Live/Dead staining of *S. aureus* biofilm on multifunctional sPEEK samples and (b) SEM observation for bacteria with and without 20 min light. Green arrows point to *S. aureus* debris, and red arrows indicate the crumpled or lytic membranes of *E. coli*.

4. CONCLUSION

In summary, by the co-functionalization of GO and APN, we have created a multi-modal therapeutic sPEEK with remotely repeatable photo-disinfection and effective osteogenicity functions. *In vitro* and *in vivo* experiments data have proved the enhanced biocompatibility, osteogenic commitment of pre-osteoblasts, and effective osteogenesis around sPEEK/GO/APN. The bactericidal tests indicate our coated samples can offer "exogenous" recyclable photothermal antimicrobial properties towards *E. coli.* and *S. aureus* without loading any antibacterial agents. Considering these results together, we demonstrate that the therapeutic PEEK materials are highly favorable for orthopedic/dental applications, especially for the treatment of BARI. Besides, such a surface engineering platform can be generalized to other medical implants/devices made of metals, ceramics, polymers, 3D printed structures, composites, etc.

ASSOCIATED CONTENT

Supporting Information

Optical images and X-ray images of rabbit femurs with different sPEEK implants after 8-week post-implantation (Figure S1); 2D micro-CT images of different implants after 4 and 8 weeks of *in vivo* implantation (Figure S2); The reusable antibacterial efficiency of samples after 1st, 2nd and 3rd cycles against *S. aureus* and *E. coli* (Figure S3); The spread plates of *S. aureus* and *E. coli*. treated with samples at 3rd cycles (Figure S4); Ion concentrations of 1X SBF (Table S1); Primer sequence (5′-3′) for the quantitative RT-PCR (Table S2)

AUTHOR INFORMATION

Corresponding Authors

*E-mail: ywz@scu.edu.cn (YWZ)

*E-mail: swallow@swmu.edu.cn (CYD)

*E-mail: zhigang.chen@usq.edu.au; zhigang.chen@uq.edu.au (ZGC)

Author Contributions

The manuscript was written through the contributions of all authors. All authors have approved the final version of the manuscript.

Funding Sources

This work is jointly funded by the National Natural Science Foundation of China (81801848, 81961160736), Sichuan Science and Technology Program (2017FZ0046, 2018JZ0026), Young Elite Scientist Sponsorship Program by CAST, Chengdu International Science and Technology Cooperation Foundation (2017-GH02-00025-HZ), State Key Laboratory of Polymer Materials Engineering (Grant No.: sklpme2019-2-05), Sichuan University Postdoctoral Interdisciplinary Innovation Foundation, Doctoral Fund of the Affiliated Hospital of Southwest Medical University (18059), Sichuan Province-Luzhou City-Southwest Medical Foundation (14JC0038), Scientific Projects of Sichuan Education Department (18ZA05193D), Australian Research Council, and USQ Strategic Research Fund. The authors would also like to thank Hui Wang, Chenghui Li, and Daibing Luo (Analytical & Testing Center, Sichuan University) for their help in SEM and CLSM, respectively.

Notes

The authors declare no competing financial interest.

REFERENCES

(1) Bose, S.; Ke, D.; Sahasrabudhe, H.; Bandyopadhyay, A., Additive Manufacturing of Biomaterials. *Prog. Mater. Sci.* **2018**, *93*, 45-111.

(2) Wang, L.; He, S.; Wu, X.; Liang, S.; Mu, Z.; Wei, J.; Deng, F.; Deng, Y.; Wei, S., Polyetheretherketone/Nano-Fluorohydroxyapatite Composite with Antimicrobial Activity and Osseointegration Properties. *Biomaterials* **2014**, *35*, 6758-6775.

(3) Hetrick, E. M.; Schoenfisch, M. H., Reducing Implant-Related Infections: Active Release Strategies. *Chem. Soc. Rev.* **2006**, *35*, 780-789.

(4) Van Oosten, M.; Schäfer, T.; Gazendam, J. A. C.; Ohlsen, K.; Tsompanidou, E.; de Goffau, M. C.; Harmsen, H. J. M.; Crane, L. M. A.; Lim, E.; Francis, K. P., Real-Time In Vivo Imaging of Invasive- and Biomaterial-Associated Bacterial Infections Using Fluorescently Labelled Vancomycin. *Nat. Commun.* **2013**, *4*, 2584.

(5) Busscher, H. J.; van der Mei, H. C.; Subbiahdoss, G.; Jutte, P. C.; van den Dungen, J. J. A. M.; Zaat, S. A. J.; Schultz, M. J.; Grainger, D. W., Biomaterial-Associated Infection: Locating the Finish Line in the Race for the Surface. *Sci. Transl. Med.* **2012**, *4*, 153rv10.

(6) Levin-Reisman, I.; Ronin, I.; Gefen, O.; Braniss, I.; Shoresh, N.; Balaban, N. Q., Antibiotic Tolerance Facilitates the Evolution of Resistance. *Science* **2017**, *355*, 826-830.

(7) Martínez, J. L., Antibiotics and Antibiotic Resistance Genes in Natural Environments. *Science* **2018**, *321*, 365-367.

(8) Ulldemolins; Marta, Antibiotic Dosing in Multiple Organ Dysfunction Syndrome. *Chest* **2011**, *139*, 1210 -1220.

(9) Jo, M., When Antibiotics Turn Toxic. *Nature* **2018**, *555*, 431-433.

(10) Xiong, M. H.; Li, Y.-J.; Bao, Y.; Yang, X.-Z.; Hu, B.; Wang, J., Bacteria-Responsive Multifunctional Nanogel for Targeted Antibiotic Delivery *Adv. Mater*. **2012**, *24*, 6175-6180.

(11) Min, J.; Choi, K. Y.; Dreaden, E. C.; Padera, R. F.; Braatz, R. D.; Spector, M.; Hammond, P. T., Designer Dual Therapy Nanolayered Implant Coatings Eradicate Biofilms and Accelerate Bone Tissue Repair. *ACS Nano* **2016**, *10*, 4441-4450.

(12) Tao, Y.; Ju, E.; Ren, J.; Qu X., Bifunctionalized Mesoporous Silica-Supported Gold Nanoparticles: Intrinsic Oxidase and Peroxidase Catalytic Activities for Antibacterial Applications. *Adv. Mater.* **2015**, *27*, 1097-1104.

(13) Chernousova, S.; Epple, M., Silver as Antibacterial Agent: Ion, Nanoparticle, and Metal. *Angew. Chem. Int. Edit.* **2013**, *52*, 1636-1653.

(14) Giano, M. C.; Ibrahim, Z.; Medina, S. H.; Sarhane, K. A.; Christensen, J. M.; Yamada, Y.; Brandacher, G.; Schneider, J. P., Injectable Bioadhesive Hydrogels with Innate Antibacterial Properties. *Nat. Commun.* **2014**, *5*, 4095.

(15) Michael; Zasloff, Antimicrobial Peptides of Multicellular Organisms. *Adv. Exp. Med. Biol* **2002**, *415*, 389-395.

(16) Hu, B.; Owh, C.; Chee, P. L.; Leow, W. R.; Liu, X.; Wu, Y.-L.; Guo, P.; Loh, X. J.; Chen, X., Supramolecular Hydrogels for Antimicrobial Therapy. *Chem. Soc. Rev.* **2018**, *47*, 6917-6929.

(17) Swartjes, J. J. T. M.; Das, T.; Sharifi, S.; Subbiahdoss, G.; Sharma, P. K.; Krom, B. P.; Busscher, H. J.; van der Mei, H. C., A Functional DNase I Coating to Prevent Adhesion of Bacteria and the Formation of Biofilm. *Adv. Funct. Mater.* **2013**, *23*, 2843-2849.

(18) Chen, Z.; Ji, H.; Liu, C.; Bing, W.; Wang, Z.; Qu, X., A Multinuclear Metal Complex Based DNase-Mimetic Artificial Enzyme: Matrix Cleavage for Combating Bacterial Biofilms. *Angew. Chem. Int. Edit.* **2016**, *55*, 10732-10736.

(19) Xie, X.; Mao, C.; Liu, X.; Lei, T.; Wu, S., Tuning the Bandgap of Photo-Sensitive Polydopamine/Ag_3PO_4/Graphene Oxide Coating for Rapid, Noninvasive Disinfection of Implants. *ACS Central Sci.* **2018**, *4*, 724-738.

(20) Wang, X.; Su, K.; Tan, L.; Liu, X.; Cui, Z.; Jing, D.; Yang, X.; Liang, Y.; Li, Z.; Zhu, S., Rapid and Highly Effective Non-invasive Disinfection by Hybrid Ag/CS@MnO_2 Nanosheets Using Near-Infrared Light. *ACS Appl. Mater. Interfaces* **2019**, *11*, 15014-15027.

(21) Yuan, Z.; Tao, B.; He, Y.; Mu, C.; Liu, G.; Zhang, J.; Liao, Q.; Liu, P.; Cai, K., Remote Eradication of Biofilm on Titanium Implant via Near-Infrared Light Triggered Photothermal/Photodynamic Therapy Strategy. *Biomaterials* **2019**, *223*, 119479

(22) Wang, C.; Wang, Y.; Zhang, L.; Miron, R. J.; Liang, J.; Shi, M.; Mo, W.; Zheng, S.; Zhao, Y.; Zhang, Y., Pretreated Macrophage-Membrane-Coated Gold Nanocages for Precise Drug Delivery for Treatment of Bacterial Infections. *Adv. Mater.* **2018**, *30*, 1804023.

(23) Hu, D.; Li, H.; Wang, B.; Ye, Z.; Lei, W.; Jia, F.; Jin, Q.; Ren, K.-F.; Ji, J., Surface-Adaptive Gold Nanoparticles with Effective Adherence and Enhanced Photothermal Ablation of Methicillin-Resistant Staphylococcus Aureus Biofilm. *ACS Nano* **2017**, *11*, 9330-9339.

(24) Tian, B.; Wang, C.; Zhang, S.; Feng, L.; Liu, Z., Photothermally Enhanced Photodynamic Therapy Delivered by Nano-Graphene Oxide. *ACS Nano* **2011**, *5*, 7000-7009.

(25) Wu, M. C.; Deokar, A. R.; Liao, J.-H.; Shih, P.-Y.; Ling, Y.-C., Graphene-Based Photothermal Agent for Rapid and Effective Killing of Bacteria. *ACS Nano* **2013**, *7*, 1281-1290.

(26) Yin, W.; Yu, J.; Lv, F.; Yan, L.; Zheng, L. R.; Gu, Z.; Zhao, Y., Functionalized Nano-MoS_2 with Peroxidase Catalytic and Near-Infrared Photothermal Activities for Safe and Synergetic Wound Antibacterial Applications. *ACS Nano* **2016**, *10*, 11000-11011.

(27) Chou, S. S.; Kaehr, B.; Kim, J.; Foley, B. M.; De, M.; Hopkins, P. E.; Huang, J.; Brinker, C. J.; Dravid, V. P., Chemically Exfoliated MoS_2 as Near-Infrared Photothermal Agents. *Angew. Chem. Int. Edit.* **2013**, *52*, 4160-4164.

(28) Cao, F.; Ju, E.; Zhang, Y.; Wang, Z.; Qu, X., An Efficient and Benign Antimicrobial Depot Based on Silver-Infused MoS_2. *ACS Nano* **2017**, *11*, 4651-4659.

(29) Wang, X.; Su, K.; Tan, L.; Liu, X.; Cui, Z.; Jing, D.; Yang, X.; Liang, Y.; Li, Z.; Zhu, S.; Yeung, K. W. K.; Zheng, D.; Wu, S., Rapid and Highly Effective Noninvasive Disinfection by Hybrid Ag/CS@MnO_2 Nanosheets Using Near-Infrared Light. *ACS Appl. Mater. Interfaces* **2019**, *11*, 15014-15027.

(30) Wu, B.; Li, Y.; Su, K.; Tan, L.; Liu, X.; Cui, Z.; Yang, X.; Liang, Y.; Li, Z.; Zhu, S.; Yeung, K. W. K.; Wu, S., The Enhanced Photocatalytic Properties of MnO_2/g-C_3N_4 Heterostructure for Rapid Sterilization under Visible Light. *J. Hazard. Mater.* **2019**, *377*, 227-236.

(31) Chen, W.; Ouyang, J.; Liu, H.; Chen, M.; Zeng, K.; Sheng, J.; Liu, Z.; Han, Y.; Wang, L.; Li, J., Black Phosphorus Nanosheet-Based Drug Delivery System for Synergistic Photodynamic/Photothermal/Chemotherapy of Cancer. *Adv. Mater.* **2017**, *29*, 1603864.

(32) Shao, J.; Xie, H.; Huang, H.; Li, Z.; Sun, Z.; Xu, Y.; Xiao, Q.; Yu, X.-F.; Zhao, Y.; Zhang, H., Biodegradable Black Phosphorus-Based Nanospheres for In Vivo Photothermal Cancer Therapy. *Nat. Commun.* **2016**, *7*, 12967.

(33) Rasool, K.; Helal, M.; Ali, A.; Ren, C. E.; Gogotsi, Y.; Mahmoud, K. A., Antibacterial Activity of $Ti_3C_2T_x$ MXene. *ACS Nano* **2016**, *10*, 3674-3684.

(34) Lin, H.; Wang, Y.; Gao, S.; Chen, Y.; Shi, J., Theranostic 2D Tantalum Carbide (MXene). *Adv. Mater.* **2018**, *30*, 1703284.

(35) Cheng, C.; Li, S.; Thomas, A.; Kotov, N. A.; Haag, R., Functional Graphene Nanomaterials Based Architectures: Biointeractions, Fabrications, and Emerging Biological Applications. *Chem. Rev.* **2017**, *117*, 1826-1914.

(36) Nie, C.; Ma, L.; Li, S.; Fan, X.; Yang, Y.; Cheng, C.; Zhao, W.; Zhao, C., Recent Progresses in Graphene Based Bio-Functional Nanostructures for Advanced Biological and Cellular Interfaces. *Nano Today* **2019**, *26*, 57-97.

(37) Chung, C.; Kim, Y. K.; Shin, D.; Ryoo, S. R.; Hong, B. H.; Min, D. H., Biomedical Applications of Graphene and Graphene Oxide. *Accounts Chem. Res.* **2013**, *46*, 2211-2224.

(38) Wang, Y.; Zhang, X.; Shao, J.; Liu, H.; Liu, X.; Luo, E., Adiponectin Regulates BMSC Osteogenic Differentiation and Osteogenesis Through the Wnt/β-catenin Pathway. *Sci. Rep.* **2017**, *7*, 3652.

(39) Lee, H. W.; Sang, Y. K.; Kim, A. Y.; Lee, E. J.; Choi, J. Y.; Kim, J. B., Adiponectin Stimulates Osteoblast Differentiation Through Induction of COX2 in Mesenchymal Progenitor Cells. *Stem Cells* **2009**, *27*, 2254-2262.

(40) Luo, E.; Hu, J.; Bao, C.; Li, Y.; Tu, Q.; Murray, D.; Chen, J., Sustained Release of Adiponectin Improves Osteogenesis Around Hydroxyapatite Implants by Suppressing Osteoclast Activity in Ovariectomized Rabbits. *Acta Biomater.* **2012**, *8*, 734-743.

(41) Wang, M.; Deng, Y.; Zhou, P.; Luo, Z.; Li, Q.; Xie, B.; Zhang, X.; Chen, T.; Pei, D.; Tang, Z., In Vitro Culture and Directed Osteogenic Differentiation of Human Pluripotent Stem Cells on Peptides-Decorated Two-Dimensional Microenvironment. *ACS Appl. Mater. Interfaces* **2015**, *7*, 4560-4572.

(42) Lee, H.; Dellatore, S. M.; Miller, W. M.; Messersmith, P. B., Mussel-Inspired Surface Chemistry for Multifunctional Coatings. *Science* **2007**, *318*, 426-430.

(43) Deng, Y.; Wei, S.; Yang, L.; Yang, W.; Dargusch, M. S.; Chen, Z.-G.; A Novel Hydrogel Surface Grafted With Dual Functional Peptides for Sustaining Long-Term Self-Renewal of Human Induced Pluripotent Stem Cells and Manipulating Their Osteoblastic Maturation. *Adv. Funct. Mater.* **2018**, *28*, 1705546.

(44) Kokubo, T.; Takadama, H., How Useful Is SBF in Predicting In Vivo Bone Bioactivity? *Biomaterials* **2006**, *27*, 2907-2915.

(45) Deng, Y.; Yang, W.-Z.; Shi, D.; Wu, M.; Xiong, X.-L.; Chen, Z.-G.; Wei, S.-C., Bioinspired and Osteopromotive Polydopamine Nanoparticle-Incorporated Fibrous Membranes for Robust Bone Regeneration. *NPG Asia Mater.* **2019**, *11*, 39.

(46) Xu, A.; Zhou, L.; Deng, Y.; Chen, X.; Xiong, X.; Deng, F.; Wei, S., A Carboxymethyl Chitosan and Peptide-Decorated Polyetheretherketone Ternary Biocomposite with Enhanced Antibacterial Activity and Osseointegration as Orthopedic/Dental Implants. *J. Mater. Chem. B* **2016**, *4*, 1878-1890.

(47) Torstrick, F. B.; Lin, A. S. P.; Potter, D.; Safranski, D. L.; Sulchek, T. A.; Gall, K.; Guldberg, R. E., Porous PEEK Improves the Bone-Implant Interface Compared to Plasma-Sprayed Titanium Coating on PEEK. *Biomaterials* **2018**, *185*, 106-116.

(48) Wang, S.; Yang, Y.; Li, Y.; Shi, J.; Zhou, J., Strontium/Adiponectin Co-Decoration Modulates the Osteogenic Activity of Nano-Morphologic Polyetheretherketone Implant. *Colloid. Surface. B* **2019**, *176*, 38-46.

(49) Kenry; Chaudhuri, P. K.; Loh, K. P.; Lim, C. T., Selective Accelerated Proliferation of Malignant Breast Cancer Cells on Planar Graphene Oxide Films. *ACS Nano*, **2016**, *10*, 3424-3434.

(50) Ouyang, L.; Zhao, Y.; Jin, G.; Tao, L.; Liu, X., Influence of Sulfur Content on Bone Formation and Antibacterial Ability of Sulfonated PEEK. *Biomaterials* **2016**, *83*, 115-126.

(51) Nayak, T. R.; Andersen, H.; Makam, V. S.; Khaw, C.; Bae, S.; Xu, X.; Ee, P.-L. R.; Ahn, J.-H.; Hong, B. H.; Pastorin, G., Graphene for Controlled and Accelerated Osteogenic Differentiation of Human Mesenchymal Stem Cells. *ACS Nano* **2011**, *5*, 4670-4678.

(52) Chen, T.; Wu, Y.; Lu, H.; Guo, Y.; Tang, Z., Adiponectin Enhances Osteogenic Differentiation in Human Adipose-Derived Stem Cells by Activating the APPL1-AMPK Signaling Pathway. *Biochem. Bioph. Res. Commun.* **2015**, *461*, 237-242.

(53) Otsuki, B.; Takemoto, M.; Fujibayashi, S.; Neo, M.; Kokubo, T.; Nakamura, T., Pore Throat Size and Connectivity Determine Bone and Tissue Ingrowth Into Porous Implants: Three-Dimensional Micro-CT Based Structural Analyses of Porous Bioactive Titanium Implants. *Biomaterials* **2006**, *27*, 5892-5900.

TOC GRAPHIC

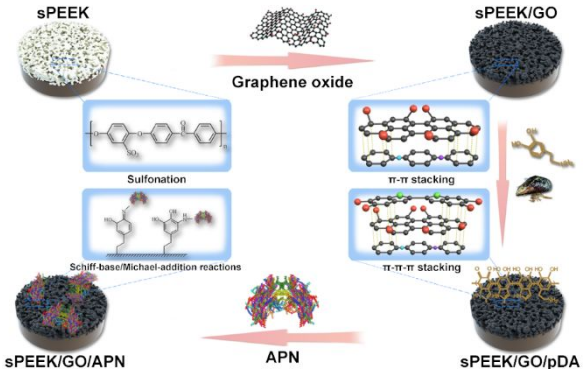
sPEEK
Graphene oxide
sPEEK/GO
Sulfonation
π-π stacking
Schiff-base/Michael-addition reactions
π-π-π stacking
sPEEK/GO/APN
APN
sPEEK/GO/pDA